Mutual Synchronization of Spin-Torque Nano-Oscillators Via Oersted Magnetic Fields Created by Waveguides

Hanuman Singh,[1] S. Bhuktare,[1] A. Bose,[1] A. Fukushima,[2] K. Yakushiji,[2] S. Yuasa,[2] H. Kubota,[2] and Ashwin A. Tulapurkar[1,*]

[1]*Department of Electrical Engineering, Indian Institute of Technology Bombay, Powai, Mumbai 400 076, India*
[2]*National Institute of Advanced Industrial Science and Technology (AIST), Spintronics Research Center, Ibaraki 305-8568, Japan*

Nanoscale oscillators based on the spin-transfer torque effect are attractive candidates for the hardware implementation of neural networks using an array of coupled oscillators. Here, we demonstrate that the mutual coupling through rf strip lines can be used for synchronizing two spin-torque nano-oscillators (STNOs). Using the current nanotechnology, it is feasible to design asymmetric coupling between two STNOs via this scheme, which would mimic many biological neural networks. A unique feature of our experiment is that we can characterize the synchronized state by varying the phase as well as the strength of the coupling, going into the nonlinear regime.

I. INTRODUCTION

The magnetization of a nanomagnet can be manipulated by the spin-transfer torque (STT) effect [1,2]. STT effect can be used to switch the magnetization as well as to drive it into continual precessional modes [3–5]. Nanoscale oscillators based on STT have been the subject of intensive research [6–10] for the past two decades due to potential applications to rf devices [11,12], and communication systems. Alternative ways of generating spin current and STT are also being explored [13,14]. Recently, spin-torque nano-oscillators (STNOs) have emerged as potential candidates for neuromorphic applications [15]. A mutually synchronized array of STNOs could be used for oscillator-based computing schemes, where the information is stored in the phase of the oscillators. Synchronization of oscillators is also important for rf applications, as the linewidth and the output power can be improved by mutual phase coupling.

The mutual synchronization of STNO was demonstrated by Kaka *et al*. [16] and Mancoff *et al*. [17] using spin-wave coupling in a point contact geometry in 2005. Later several groups studied the synchronization process [18–31] using coupling via spin waves [32,33] or dipolar interaction [34] in different geometries. A long-range electrical coupling scheme has been used to synchronize vortex-based oscillators recently [35]. Here, we demonstrate mutual synchronization of in-plane magnetized, magnetic-tunnel-junction- (MTJ) based STNO by coupling via Oersted

magnetic field [36,37]. The coupling arises as follows: each MTJ is connected to a waveguide, which is located on top of the other MTJ. A small part of the rf-voltage output of one oscillator is used to generate rf current through the waveguide, which exerts Oersted magnetic field on the other oscillator. This results in a coupling between them. In this scheme of coupling, the two oscillators can be far away (few mm) as the rf current can be carried by long waveguides. Our results show that we can improve the power output as well as the linewidth by synchronization. A feature of our experiment is that we control both the phase and strength of the coupling. A further interesting point is that a strong coupling itself can generate the oscillatory state, which has been demonstrated previously [37]. We indeed observe nonlinear effects as we increase the coupling strength: the power spectrum develops a sharp peak with side bands.

II. SAMPLE PREPARATION AND EXPERIMENTAL SETUP

The MTJ stack is fabricated on a thermally grown SiO_2 (500 nm) with the following structure: bottom contact (50 nm)/Ta (5 nm)/IrMn (7 nm)/CoFe (2.5 nm)/Ru (0.82 nm)/(Co, Fe)B (1 nm)/Ta(0.3 nm)/(Co, Fe)B (1.5 nm) /CoFe (0.5 nm)/MgO (0.9 nm)/(Co, Fe)B (1.8 nm)/Ta (5 nm)/Ru (7 nm)/top contact (45 nm). The Ta insertion layer keeps the fourfold symmetry, that is (001)-oriented texture, for the (Co, Fe)B/MgO part after high-temperature annealing. Elliptical nanopillars of sizes 210×70 nm^2 and 150×50 nm^2 from above the multilayer

*ashwin@ee.iitb.ac.in

stack are fabricated using e-beam lithography and Ar ion milling. For magnetic field coupling, on top of each MTJ nanopillar, a coplanar waveguide (CPW) of width 2 μm and electrically insulated from the MTJ is fabricated. The easy axis direction of the free layer along the direction of the x axis and the fixed layer is oriented at 45° with respect to the x axis. The CPW orientation is such that current passing through it produces a magnetic field along 45° with respect to the x axis. All the experiments are performed at room temperature.

The schematic of the experimental setup to study the mutual synchronization of two STNOs with magnetic field coupling is shown in Fig. 1. The two MTJs are powered by two separate dc-current sources with two bias tees. The rf output of MTJ1 (2) is split into two parts: one part is used for measuring output and the other part is amplified and fed to the waveguide on top of the MTJ2 (1). The outputs from the two MTJs, which are to be used for measuring the output, are combined together and fed to a spectrum analyzer. In the experiment, we also add two isolators before combining the two signals, one between splitter 1 and the adder, and the other between splitter 2 and the adder. These are not shown in Fig. 1. This avoids direct electrical coupling between the two MTJs and also self-injection locking [31]. The lengths of the two coupling paths are nominally the same. Similarly, the lengths of the two measurement paths are also nominally the same. Adjustable delay (phase shifter) is inserted in the coupling path of MTJ2 to MTJ1 as shown in Fig. 1. As the two MTJs are kept far away from each other (approximately 1 m), we use two electromagnets to apply different magnetic fields to them. Our setup also allows us to characterize the power output from each MTJ separately without coupling between them. The mutual synchronization works as follows: dc current is passed through both the MTJs to

set them into oscillatory state by the STT effect. The rf output of MTJ1 passes rf current through the waveguide on top of MTJ2 and creates rf magnetic field on MTJ2. This gives rise to a coupling between MTJ2 and 1. Similarly, the rf output of MTJ2 creates rf magnetic field on MTJ1, which gives rise to a coupling between MTJ1 and 2. If the free-running oscillation frequencies of the two MTJs are close by, they can synchronize and oscillate with the same frequency. In our experiment, we pass fixed dc currents through both the MTJs and apply a fixed magnetic field to MTJ1. The magnetic field applied to MTJ2 is varied to vary the free-running oscillation frequency of MTJ2.

In our setup, there are two amplifiers: one in the coupling path for each MTJ. The gains of the amplifiers are controlled by dc bias current. We adjust the bias currents to the amplifiers such that both of them have approximately the same gain. We carry out synchronization measurements for different values of the amplifier gains by changing the bias currents to the amplifiers. Thus our setup allows synchronization to be studied as a function of the coupling strength. This was not possible in the previous experiments on synchronization. (We also carry out measurements without any amplifier and verify that synchronization is possible. The advantage of inserting amplifiers is that we can explore the coupling strength dependence of the locking range.) Further, the phase shifter in the coupling path allows us to study the effect of coupling phase on the synchronized state.

III. RESULTS AND DISCUSSION

A 2D plot of the combined power spectral density (PSD) as a function of frequency and magnetic field applied to MTJ2 (H_2) is shown in Fig. 2(a) (the color bar is in log scale). Bias currents of 1.4 mA are applied to each MTJ.
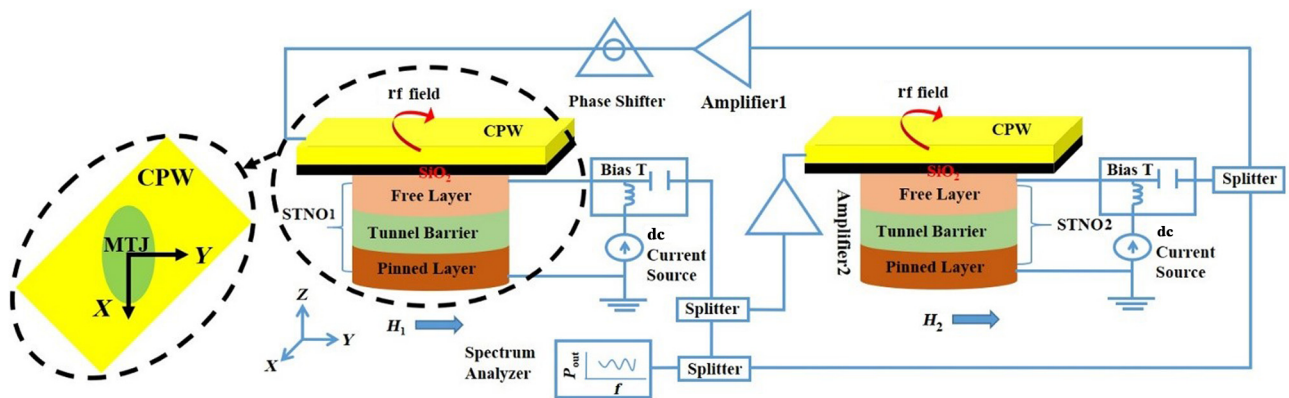

FIG. 1.   Schematic diagram for the mutual synchronization of two spin-torque nano-oscillators with Oersted magnetic field coupling. Both the MTJs comprise free layer, tunnel barrier, and pinned layer. A CPW is situated on the top of each MTJ, which is electrically insulated from MTJs. Both MTJs are independently biased by passing dc currents through bias tees. The rf output signals generated are split into two parts using a power splitter. One part is amplified and fed back to the CPW of the other MTJ. The amplified output current passing through the CPW creates the coupling microwave magnetic fields, which gives rise to synchronization. The second parts of output signals are combined and observed on a spectrum analyzer.
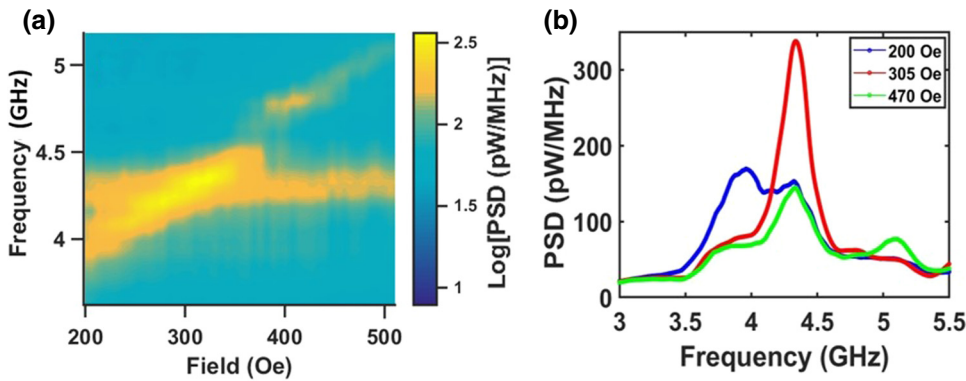
FIG. 2. Experimental results. (a) 2D color plot (in log scale) of the power spectral density as a function of the magnetic field applied to MTJ2 and frequency. Magnetic field applied to MTJ1 is 300 Oe. (b) Projections of the 2D plot at $H_2 = 200$, 305, and 470 Oe. The oscillators are synchronized at $H_2 = 305$ Oe and, unsynchronized at 200 and 470 Oe.

Magnetic field of 300 Oe is applied to MTJ1. The amplifier gains are set to 15 dB. One-dimensional projections of Fig. 2(a), at $H_2 = 200$, 305, and 470 Oe are shown in Fig. 2(b).

From Fig. 2(a), we can see that in a certain range of H_2, (when the free-running frequencies are close by) the out power is enhanced, which corresponds to the synchronization of the two STNOs. The phase shifter in the coupling path between STNO2 to STNO1 is adjusted to a phase of approximately 50° to get the brightest spot. The synchronization can also be seen from Fig. 2(b): at $H_2 = 305$ Oe, the spectrum shows a single peak with large amplitude, which indicates synchronization. At $H_2 = 200$ and 470 Oe, the two STNOs are not synchronized and two peaks at two different frequencies can be seen. The spectra shown in Fig. 2(b) are fitted to the Lorentzian curve near the peak region to extract linewidth and power. In the case of spectra with two peaks, both are fitted simultaneously.

The integrated output power as a function of H_2 is shown in Fig. 3(a). Blue and green curves show the power of the uncoupled state of oscillators 1 (P_{STNO1}) and 2 (P_{STNO2}), respectively. Dark green and magenta curves show the power of the free-running oscillator 1 [$P_{(STNO1)freerunning}$] and the power of free-running oscillator 2 [$P_{(STNO2)freerunning}$], respectively. The free-running power is measured with biasing only one MTJ and setting the amplifier gain to 0. The dark gray curve shows

the sum and the orange curve shows twice the sum of the powers of free-running oscillators. The red curve shows the power of the coupled oscillator system. The fact that the red curve lies between dark gray curves, shows that the oscillator system is coupled with a phase difference between 0° to 90°. If the two oscillators are uncoupled, we would get an incoherent sum of their powers, i.e., $P_{STNO1freerunning} + P_{STNO2freerunning}$. Figure 3(b) shows the linewidth as a function of H_2. We can see that in the synchronized regime, power increases and the linewidth decreases. The improvement in power and reduction in linewidth is discussed in the Appendix.

It can be seen from Fig. 3(b) that the linewidth of the free STNO shows a nonmonotonic behavior. The linewidth of STNO depends on the factor $(1 + v^2)$, where v is the nonlinear dimensionless frequency-shift coefficient [6]. The observed nonmonotonic linewidth behavior can arise from the variation of v with magnetic field. Such a behavior is also seen in Ref. [38] and explained in terms of v. It can also be seen from Fig. 3(a) that the power output of STNO2 outside the mutual synchronization regime is higher than its free-running power. The STNO1 has somewhat higher free-running power and this may be affecting the STNO2 even outside the synchronization regime.

Next, we study the effect of coupling phase on synchronization. We vary the phase of coupling between STNO2 to STNO1 by using the phase shifter shown in Fig. 1, while
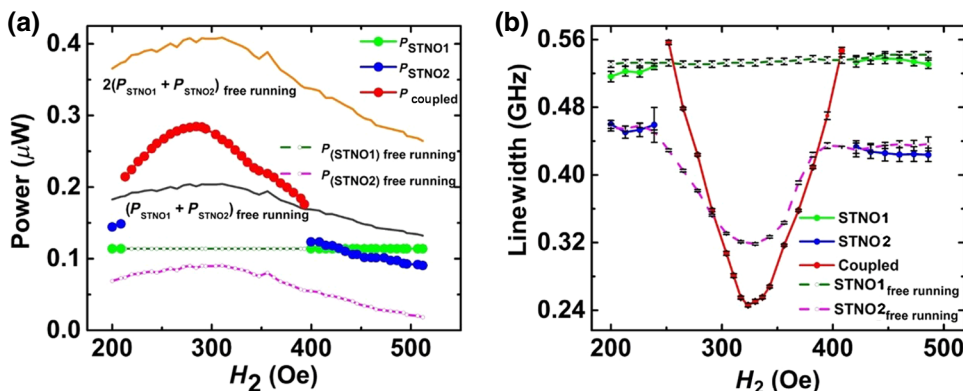

FIG. 3. Experimental results. (a) The integrated power of STNOs in coupled and uncoupled states and individual power of the two separate STNOs. (b) The variation of linewidth of combined spectra for oscillators in coupled and uncoupled states and the linewidth of individual oscillator STNO1 with magnetic field from 190 to 510 Oe. Magnetic field applied to STNO2 is varied, keeping the magnetic field applied to STNO1 constant.
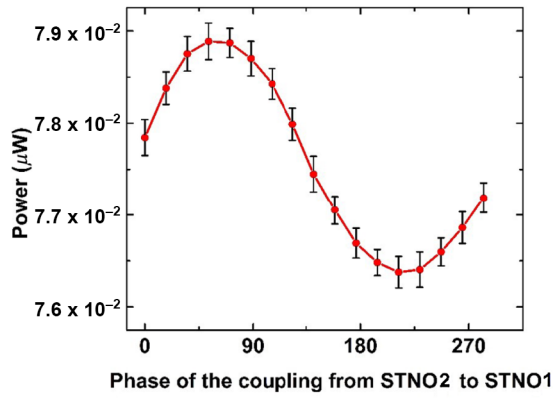
FIG. 4.   Experimental results. The variation of power in the synchronized state as a function of the coupling phase. The phase is varied only in one path: from STNO2 to STNO1. The solid line is a guide to the eye.

keeping the phase of coupling between STNO1 to STNO2 constant. Figure 4 shows the variation of power as a function of phase of the coupling signal. These measurements are carried out on a sample different from the previous one. These samples are on the same wafer with the same nominal dimensions and fabricated simultaneously. However, the spin-torque efficiency is lower than the previous samples. The magnetic field on MTJ2 is adjusted so that free-running frequencies of the oscillators are almost equal for this measurement. We can see a clear oscillation in the power as a function of the coupling phase. However, the relative power variation is quite small. Using the theory developed in Ref. [6], we expect to see a large power variation (minimum power would be zero for two identical oscillators with the same coupling) with sudden jumps as a function of phase. It is shown in the Appendix that the thermal fluctuations smoothen and lower the relative power variation. The simulation of the free-layer magnetization dynamics by the Landau-Lifshitz-Gilbert (LLG) equation (simplified to include only dampinglike torque) also qualitatively supports this behavior. We therefore claim that thermal fluctuations have a crucial influence on the power modulation as a function of the coupling phase.
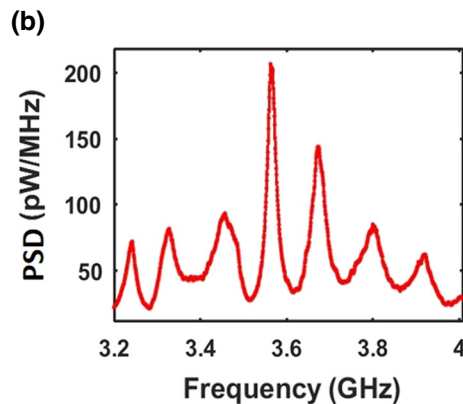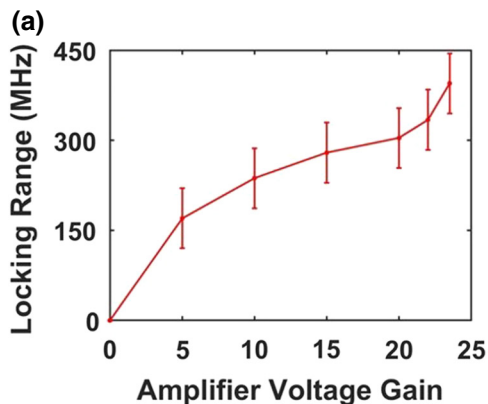
Next we carry out synchronization measurements for various values of the amplifier gains keeping the coupling phase constant. The mutual phase locking range as a function of the amplifier gain is plotted in Fig. 5(a). The linear dependence of locking range observed for low gains (approximately 15 dB) is expected from the theory of mutual synchronization [6]. The LLG-equation simulations also support the theory. For higher amplifier gain, the locking range shows nonlinear dependence. This behavior is also qualitatively supported by the LLG-equation simulation. As we increase the gain, the oscillator system is no longer a weakly coupled system. In fact, for large gain, the coupling itself can lead to an oscillatory state of the combined system of two MTJs, i.e., even if the STT effect is absent (e.g., we can make the STT effect very small by increasing the thickness of the free layers) the coupling between the MTJs can drive them into oscillatory state. This is shown for the case of a single MTJ in Ref. [37]. The power spectrum obtained at higher gain is shown in Fig. 5(b). One can see that the spectrum shows a sharp center peak with many side-band peaks, whose separation depends on the coupling delay. The coupling delay is about 8 ns in our setup, which corresponds to a frequency separation of about 120 MHz. (This situation can be compared to the case of lasers: the cavity delay gives rise to a similar side-peak spectrum.) This is a signature that the coupling is playing a dominant role in the dynamics. The mutual phase locking range in this regime increases sharply with gain. The LLG simulations agree with the experimental observation of side-band peaks for higher gain (results not shown).

IV. NUMERICAL SIMULATION

We carry out numerical simulation of the synchronization process using the LLG equations given below:

$$\dot{\hat{m}}_1 = -\gamma \hat{m}_1 \times (\bar{H}_{\text{eff1}} + \bar{h}_{r1} + \bar{h}_{fb2}) + \alpha(\hat{m}_1 \times \dot{\hat{m}}_1)$$

$$+ \frac{1}{qN_{s1}}(\hat{m}_1 \times \bar{I}_{s1} \times \hat{m}_1), \tag{1a}$$

FIG. 5.   Experiment. (a) Amplifier voltage gain vs mutual phase locking range. (b) The PSD of the coupled oscillator with higher amplification.
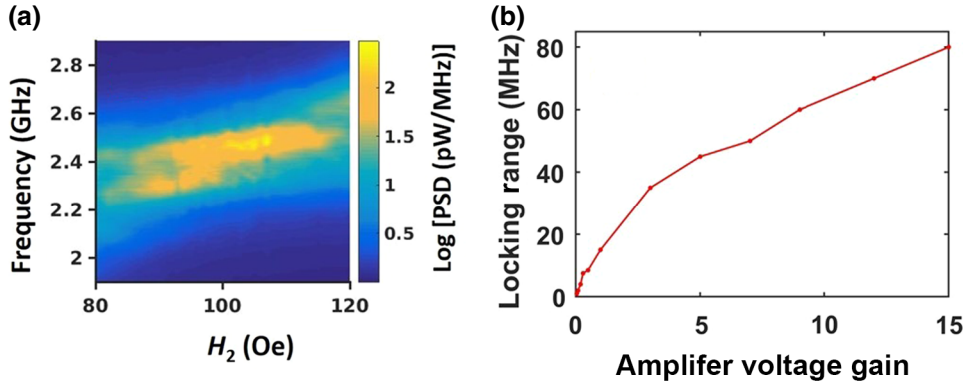
(a)

(b)

FIG. 6. Macromagnetic simulation results. (a) Color plot (in log scale) shows the PSD of mutually coupled STNOs with variation of magnetic field applied to the MTJ2 from 80 to 120 Oe. The magnetic field applied to the MTJ1 is fixed at 100 Oe. The results are obtained at 300 K. (b) Amplifier voltage gain vs mutual phase locking range for delay value of 4 ns.

$$\dot{\hat{m}}_2 = -\gamma \hat{m}_2 \times (\bar{H}_{\text{eff2}} + \bar{h}_{r2} + \bar{h}_{fb1}) + \alpha(\hat{m}_2 \times \dot{\hat{m}}_2)$$
$$+ \frac{1}{qN_{s2}}(\hat{m}_2 \times \bar{I}_{s2} \times \hat{m}_2), \tag{1b}$$

where $\hat{m}_1$, $\hat{m}_2$ represent the unit vectors along the free-layer magnetization directions of the two MTJs, γ denotes the gyromagnetic ratio, $\bar{H}_{eff\,1}$, $\bar{H}_{eff\,2}$ are the total effective magnetic fields comprising the external fields and the anisotropy fields, $\bar{h}_{r1}$, $\bar{h}_{r2}$ are the random magnetic fields originating from the thermal fluctuations of the free-layer magnetization direction, $\bar{h}_{fb1}$, $\bar{h}_{fb2}$ are the feedback (coupling) magnetic fields, which give rise to the coupling between the two MTJs. α is the Gilbert damping constant. I_{s1}, I_{s2} denotes the spin current and is given by $\bar{I}_{s1,2} = \{P_{1,2}/[1 + P_{1,2}^2(\hat{m}_{1,2}.\hat{m}_{\text{pin1,2}})]\}I_{dc1,2}\hat{m}_{\text{pin1,2}}$, where $P_{1,2}$ denotes the polarization of ferromagnet. N_{s1}, N_{s2} denotes the total number of spin given by, $N_{s1,2} = M_{s1,2}V_{1,2}/\mu_B$, where $M_{s1,2}$ denotes saturation magnetization, $V_{1,2}$ denotes the volume of free layer, and μ_B denotes Bohr magneton. The last term in the above equation gives rise to STT oscillations. The random magnetic field $h_{r1,2}$ follows the statistical properties:

$$\langle h_{r1,2,i}(t) \rangle = 0, \langle h_{r1,2,i}(t)h_{r1,2,j}(s) \rangle = 2D_{1,2}\delta_{ij}\delta(t-s),$$

$$D_{1,2} = \frac{\alpha k_B T}{\gamma_0 \mu_0 M_{s1,2} V_{1,2}}.$$

where k_B is Boltzmann's constant, T is the temperature, μ_0 is the vacuum permeability.

The feedback magnetic field acting on MTJ1 is produced as the resistance of MTJ2 is oscillating. The ac voltage produced across MTJ2 at time t is taken as $V_{ac} = I_{dc,2} * [R_2(t) - R_{0,2}]$, where $I_{dc,2}$ is the dc current passing through MTJ2, $R_2(t)$ and $R_{2,0}$ are the resistances of MTJ2 at time t and average resistance, respectively. The ac current flowing through the CPW is given by $I_{ac} = V_{ac}/(R_{0,2} + R_T)$, where R_T is the termination resistance (50 Ω). The magnetic field produced is $h_{fb,1} = I_{ac}/2w_1$, where w_1 is the width of CPW1. Because of the delay in the circuit, the magnetic field at time t is

taken as $h_{fb,1}(t) = I_{ac}(t - \Delta t)/2w_1$. The field is multiplied by amplifier gain. The feedback magnetic field acting on MTJ2 can be obtained from similar arguments.

The feedback field $h_{fb1,2}$ is taken to be along 45° from the x direction and is given by

$$h_{fb1,2}(t) = A_{1,2}I_{dc2,1}[R_{2,1}(t - \Delta t)$$
$$- R_{02,1}]/[2w_{1,2}(R_{02,1} + R_T)], \tag{2}$$

where $A_{1,2}$ is the amplifier gain.

The various parameters used in the simulation are as follows: $\alpha = 0.01$, $\gamma = 2.21 \times 10^5$ m/As, $T = 300$ K, $M_s = 10^6$ A/m, $V = (210 \times 70 \times 2 \text{ nm}^3)$, $P = 0.4$. The anisotropy magnetic field is given by $H_{\text{ani}} = H_{//}m_x - H_\perp m_z$, where $H_{//}$ and $H_\perp$ denote the in-plane and out-of-plane anisotropy fields. Positive values of $H_{//}$ and $H_\perp$ imply that the x axis is the easy axis and the z axis is the out-of-plane hard axis. We use $H_{//} = 50$ Oe and $H_\perp = 10^4$ Oe. The width of the feedback strip is taken as 1 μm and the coupling delay is taken to be $\Delta t = 8$ ns. The simulations are carried out for different values of amplifier gain.

Figure 6(a) shows the simulation results with conditions similar to the experimental conditions, i.e., magnetic field applied to the MTJ2 is varied, keeping all other parameters fixed (the color bar is in log scale). The simulation results are qualitatively similar to the experimental results plotted in Fig. 2. We also find the mutual locking range from the simulations as a function of the amplifier gain. The results shown in Fig. 6(b) have similar trends as in the experimental data in Fig. 5(a). We use macromagnetic calculations instead of micromagnetic calculations due to the small dimensions of the free layer (thickness and lateral size) [39]. We also exclude the fieldlike term from the Eqs. (1a) and (1b). Micromagnetic simulations and inclusion of the fieldlike term could give rise to better quantitative agreement with experiment. Any excitation of the pinned layer magnetization is neglected.

V. CONCLUSION

In conclusion, we show the mutual synchronization of spin-torque nano-oscillators using Oersted magnetic

field coupling generated via rf strip lines. Our experimental setup allows us to explore the synchronization phenomenon as a function of the coupling strength as well as phase. An advantage of this scheme is that it is long range, and the direction and magnitude of the coupling magnetic field on each STNO can be designed independently, by choosing the width and orientation of the CPW. (In a realistic implementation of this scheme, the coupling could be adjusted by the width of CPW rather than amplifier gain.) As an example, it is possible to go from a bidirectional coupling to a unidirectional coupling. This freedom can lead to an alternative architecture of mutually coupling an array of oscillators (see further discussion in the Supplemental Material [40], Fig. S2). Indeed, different types of interactions lead to asymmetrical coupling between biological neurons [41], which could be mimicked by the present coupling scheme. In our experiment, we use amplifiers to reach the high-coupling regime. The coupling lines in our experiment have widths of 2 μm, whereas the MTJs have diameters of approximately 100 nm. If we reduce the widths to about 100 nm, the coupling Oersted field would increase ten times. Further, the coupling can be enhanced by increasing the dc bias currents. It can be seen from Eq. (2), that the coupling magnetic field is proportional to dc current. (However, increasing the bias current could lead to a reduced nonlinear frequency-shift parameter [6], which would reduce the mutual locking range.) Thus, we can achieve strong coupling between STNOs without using amplifiers.

APPENDIX: DISCUSSION USING THE UNIVERSAL OSCILLATOR MODEL

Here, we discuss the results using the universal oscillator model developed in Ref. [6]. In the synchronized state, we consider only the dynamics of the phases of the two oscillators, which is given by

$$\dot{\phi}_1 = -\omega_{1,0} + \tilde{\Omega}_{12}\sqrt{\frac{p_{2,0}}{p_{1,0}}}\sin(\beta_{12} + \psi - \theta_1), \quad \tan\theta_1 = \nu_1$$

$$\dot{\phi}_2 = -\omega_{2,0} + \tilde{\Omega}_{21}\sqrt{\frac{p_{1,0}}{p_{2,0}}}\sin(\beta_{21} - \psi - \theta_2), \quad \tan\theta_2 = \nu_2,$$

where $\psi = \phi_2 - \phi_1$ denotes the phase difference, ω_0 denotes the free running frequency, Ω denotes the coupling

strength, p_0 denotes free-running power, β denotes the coupling phase, and ν denotes the dimensionless nonlinear frequency shift. Assuming two almost identical oscillators and adding noise terms, we can write

$$\dot{\phi}_1 = -\omega_{1,0} + \tilde{\Omega}\sin(\tilde{\beta} + \psi) + g_{11}F_1 \qquad \text{(A1)}$$

$$\dot{\phi}_2 = -\omega_{2,0} + \tilde{\Omega}\sin(\tilde{\beta} - \psi) + g_{22}F_2 \qquad \text{(A2)}$$

$$\langle F_i(t)F_j(t')\rangle = 2D\delta_{i,j}\delta(t-t'), D = 1,$$

where $\tilde{\beta} = \beta - \theta$ is the renormalized coupling phase. F_1 and F_2 denote random forces, and the coefficients g_{11} and g_{22} are constants independent of the phases. In the absence of coupling (i.e., free-running case), the random force gives rise to the broadening with linewidth $(FWHM) = 2Dg_{ii}^2$. We can write equations for the phase difference ψ and the average phase $\Phi = (\phi_1 + \phi_2)/2$ as

$$\dot{\psi} = (\omega_{1,0} - \omega_{2,0}) - 2\tilde{\Omega}\sin\psi\cos\tilde{\beta} + g_{11}\text{“}F_1\text{”} \qquad \text{(A3)}$$

$$\dot{\Phi} = -\frac{(\omega_{1,0} + \omega_{2,0})}{2} + \tilde{\Omega}\sin\tilde{\beta}\cos\psi + g_{22}\text{“}F_2\text{”} \qquad \text{(A4)}$$

where $g'_{11} = \sqrt{(g_{11}^2 + g_{22}^2)}, g'_{22} = \frac{\sqrt{(g_{11}^2 + g_{22}^2)}}{2}, \langle F'_i(t)F'_j(t')\rangle = 2D\delta_{i,j}\delta(t-t'), D = 1.$

We are interested in finding out the average value of $\cos(\psi)$ as it determines the power $[P_{tot} = 2p(1 + \cos\psi)]$. We can use the above Langevin equations to find out the average values of various quantities using the following equation [42]:

$$\text{Langevin equation:}\frac{dx_i}{dt} = h_i(\bar{x}, t)$$

$$+ \sum_j g_{i,j}(\bar{x}, t)F_j(t), \langle F_i(t)F_j(t')\rangle = 2D\delta_{i,j}\delta(t-t'),$$

$$\Rightarrow \frac{\partial\langle f(\bar{x})\rangle}{\partial t} = \sum_i\left\langle h_i\frac{\partial f}{\partial x_i}\right\rangle + \sum_{i,k,j}\left\langle Dg_{k,j}\frac{\partial}{\partial x_k}\left(g_{i,j}\frac{\partial f}{\partial x_i}\right)\right\rangle.$$

$$\text{(A5)}$$

If we put $f(\psi,\Phi) = \psi$, and $f(\psi,\Phi) = \cos(\psi)$, we get

$$\frac{\partial\langle\psi\rangle}{\partial t} = (\omega_{1,0} - \omega_{2,0}) - 2\tilde{\Omega}\cos\tilde{\beta}\langle\sin\psi\rangle$$

$$\frac{d\langle\cos\psi\rangle}{dt} = -(\omega_{1,0} - \omega_{2,0})\langle\sin\psi\rangle$$

$$+ 2\tilde{\Omega}\cos\tilde{\beta}\langle\sin^2\psi\rangle - Dg^2\langle\cos\psi\rangle.$$

Putting the left-hand sides of the above equation to 0, we get

$$\langle\sin\psi\rangle = \frac{(\omega_{1,0} - \omega_{2,0})}{2\tilde{\Omega}\cos\tilde{\beta}} \qquad \text{(A6)}$$

$$Dg^2\langle\cos\psi\rangle - 2\tilde{\Omega}\cos\tilde{\beta}\langle\sin^2\psi\rangle = -\frac{(\omega_{1,0} - \omega_{2,0})^2}{2\tilde{\Omega}\cos\tilde{\beta}}.$$

$$(A7)$$

Assuming $\psi \sim 0$, and putting $\cos\psi \sim 1 - \psi^2/2$, $\sin\psi \sim \psi$ in the above equation, we get

$$\langle\cos\psi\rangle \approx 1 - \frac{1}{2}\left[\frac{(\omega_{1,0} - \omega_{2,0})}{2\tilde{\Omega}\cos\tilde{\beta}}\right]^2 - \frac{g^2}{2\tilde{\Omega}\cos\tilde{\beta}}. \quad (A8)$$

Whereas assuming $\psi \sim \pi$, we get

$$\langle\cos\psi\rangle \approx -1 + \frac{1}{2}\left[\frac{(\omega_{1,0} - \omega_{2,0})}{2\tilde{\Omega}\cos\tilde{\beta}}\right]^2 - \frac{g^2}{2\tilde{\Omega}\cos\tilde{\beta}}. \quad (A9)$$

Note that the stability criteria requires $\cos\tilde{\beta}$ to be positive (negative) for the $\psi \sim 0$ ($\psi \sim \pi$) solution. This ensures that $|\langle\cos\psi\rangle| \leq 1$. [The above equations would not be valid if the value of g^2 (i.e., linewidth) is very large, as $|\langle\cos\psi\rangle|$ can exceed 1. This means that the assumption of $\psi \sim 0$ or π is not valid.] Equations (A8) and (A9) show that amplitude of power modulation with the phase ($\tilde{\beta}$) is reduced due to the noise. We have numerically solved Eqs. (A1) and (A2), assuming $\tilde{\Omega} = 2\pi*50$ MHz, $\omega_{1,0} = 2\pi*3$ GHz, $\omega_{2,0} - \omega_{1,0} = 2\pi*10$ MHz and $g_{11} = g_{22}$ (i.e., the same linewidth for both oscillators). The power as

a function of phase ($\tilde{\beta}$) is plotted in Figs. 7(a) and 7(b) for different values of linewidth of the free-running oscillators, i.e., different levels of noise. One can see that the sharp transition for low noise and a sinusoidal-like dependence with lower amplitude as noise is increased. This behavior matches with the experimental data shown in Fig 4. The red curve in Fig. S4(b) shows the $(1 + \langle\cos\psi\rangle)/2$ with value of $\langle\cos\psi\rangle$ given by Eqs. (A8) and (A9). The region between dotted vertical lines in Fig. S4(a), corresponds to $|\cos\tilde{\beta}| < (\omega_{1,0} - \omega_{2,0})/2\tilde{\Omega}$ where synchronization is lost [see Eq. (A6)]. The amplitude of power modulation (i.e., $P(\tilde{\beta} = 0) - P(\tilde{\beta} = \pi)$ is plotted as a function of linewidth of the free-running oscillator in Fig. 7(c). The expected linear dependence at low linewidths obtained from Eqs. (A8) and (A9) is shown by the red line in Fig. 7(c).

From Eqs. (A3)–(A5), and putting $f(\psi, \Phi) = \Phi$, and $f(\psi, \Phi) = \Phi^2$, we get

$$\frac{\partial\langle\Phi\rangle}{\partial t} = -\frac{(\omega_{1,0} + \omega_{2,0})}{2} + \tilde{\Omega}\sin\tilde{\beta}\langle\cos\psi\rangle, \quad (A10)$$

$$\frac{\partial\langle\Phi^2\rangle}{\partial t} = -(\omega_{1,0} + \omega_{2,0})\langle\Phi\rangle$$
$$+ 2\tilde{\Omega}\sin\tilde{\beta}\langle\Phi\cos\psi\rangle + 2Dg_{22}'^2. \quad (A11)$$

(a)

(b)

(c)
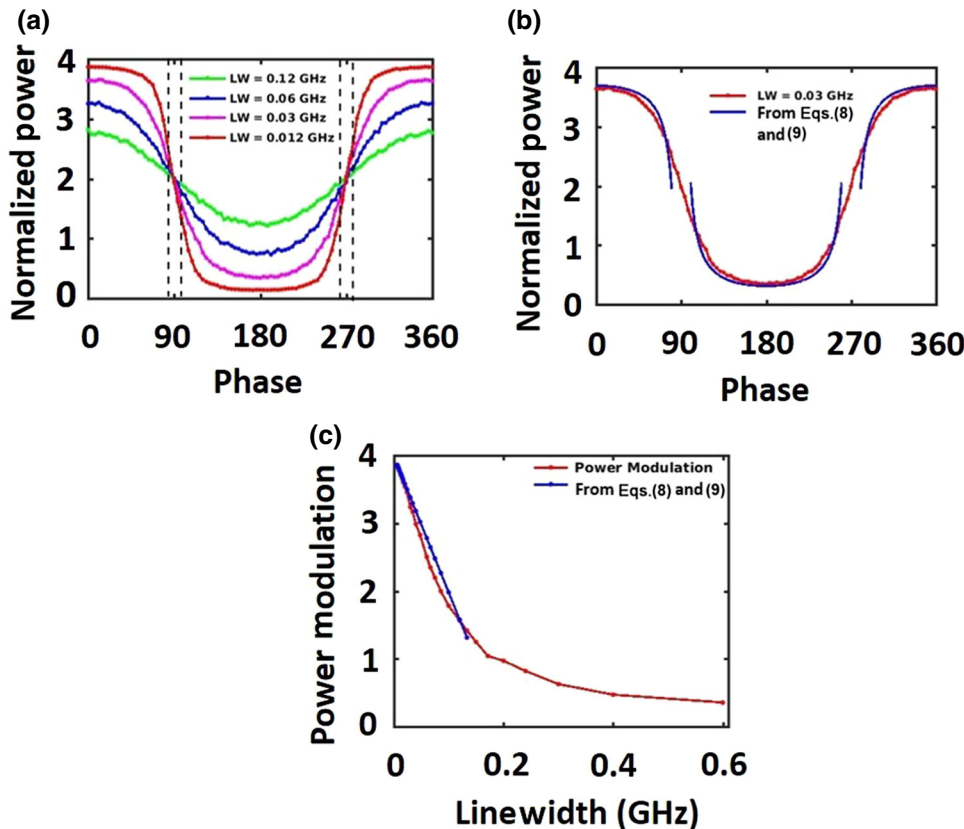
FIG. 7. (a) Normalized power obtained from numerical solution of Eqs. (A1) and (A2), as a function of phase ($\tilde{\beta}$) for different values of linewidth of the free-running oscillators. Synchronization is lost in the region between dotted lines. (b) Blue curve shows power obtained from Eqs. (A8) and (A9). (c) Red curve shows the power modulation obtained from numerical solution of Eqs. (1) and (2). Blue curve is obtained from Eqs. (A8) and (A9).

From Eq. (A10), we see that the frequency of oscillation can be different from the average frequencies of uncoupled oscillators, due to the second factor on the rhs. This factor depends on the $\langle \cos \psi \rangle$, i.e., it has the same variation as power. We can use the experimentally obtained power dependence on phase (Fig. 4) to find out the expected frequency variation as a function of phase. The coupling strength ($\tilde{\Omega}$) can be obtained from the mutual locking bandwidth. The estimated frequency variation in about 4 MHz. We are however unable to detect it clearly due to the large linewidth in our experiment.

Equation (A11) gives information about phase noise. It however requires the average value of $\Phi \cos \psi$, which is not easy to find. If the phase $\tilde{\beta}$ is 0 (maximum power) or π (minimum power), this term drops out, in which case Eq. (A11) describe the phase diffusion. Thus the linewidth of the coupled oscillator system (neglecting the amplitude noise [see Eq. (A3)], is given by LW $= 2D(g'_{22})^2 = 2D(g_{11}^2 + g_{22}^2)/4 = (LW_1 + LW_2)/4$, where LW_1 and LW_2 are the linewidths of the uncoupled oscillators. Thus the mutual synchronization gives rise to the reduction in the linewidth. If both the oscillators have equal free-running linewidths, the linewidth in the synchronized state is half of the uncoupled linewidth. This result holds for phase $= 0$ or π, i.e., even if the oscillators are synchronized in opposite phases (i.e., minimum power), the linewidth is still improved.

In our experiment, we have improvement in the linewidth in the synchronized regime as shown in Fig. 3(b). We have $LW_1 = 520$ MHz, $LW_2 = 320$ MHz for the free-running state and the minimum linewidth of the coupled state is 240 MHz. The expected linewidth of the coupled state $(LW_1 + LW_2)/4$ comes out to be 210 MHz. The higher value of observed linewidth could be due to the amplitude noise.

In the above analysis we assume that the phases of both couplings are the same. However, in the experiment we only vary the phase between oscillator 2 and 1, keeping the other phase constant. To match the experiments, we numerically solve the following equations:

$$\dot{\phi}_1 = -\omega_{1,0} + \tilde{\Omega} \sin(\tilde{\beta}_1 + \psi) + g_{11}F_1, \qquad (A12)$$

$$\dot{\phi}_2 = -\omega_{2,0} + \tilde{\Omega} \sin(\tilde{\beta}_2 - \psi) + g_{22}F_2 \qquad (A13)$$

$$\langle F_i(t)F_j(t') \rangle = 2D\delta_{i,j}\delta(t - t'), D = 1.$$

The power variation as a function of $\tilde{\beta}_2$ is shown in Fig. 8 assuming $\tilde{\Omega} = 2\pi * 50$ MHz, $\omega_{1,0} = 2\pi * 3$ GHz, $\omega_{2,0} - \omega_{1,0} = 2\pi * 10$ MHz and linewidth $= 0.12$ GHz (the same linewidth for both oscillators). The green curve is obtained with $\tilde{\beta}_1 = \tilde{\beta}_2$ and is the same as the green curve in Fig. 7(a). The red curve is obtained with $\tilde{\beta}_1 = 0$. One can see that the power modulation is reduced by half. It
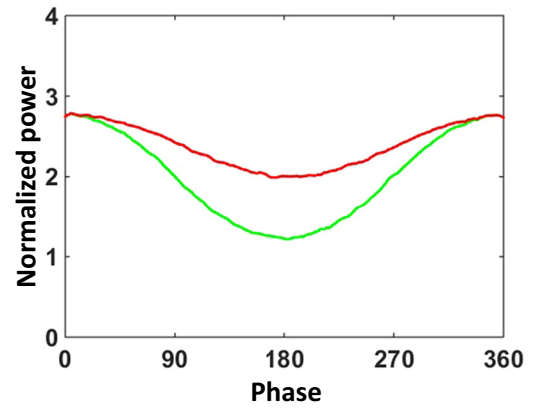

FIG. 8.   The power variation as a function of phase of the coupling between oscillators 2 and 1 ($\tilde{\beta}_2$). The green curve is obtained with $\tilde{\beta}_1 = \tilde{\beta}_2$, whereas the red curve is obtained with $\tilde{\beta}_1 = 0$.

was found that the power modulation is reduced by half for any other fixed value of $\tilde{\beta}_1$ as well. The experimentally observed power modulation is small and is a result of both changing phase of only one path and thermal fluctuations. Also the thermal fluctuations make the power variation smooth (sinusoidal looking) even when the phase of only one path is changed, which matches with the experimental observation.

[1] J. C. Slonczewski, Current-driven excitation of magnetic multilayers, J. Magn. Magn. Mater. **159**, L1 (1996).

[2] L. Berger, Emission of spin waves by a magnetic multilayer traversed by a current, Phys. Rev. B **54**, 9353 (1996).

[3] M. Tsoi, A. G. M. Jansen, J. Bass, W.-C. Chiang, V. Tsoi, and P. Wyder, Generation and detection of phase-coherent current-driven magnons in magnetic multilayers, Nature **406**, 46 (2000).

[4] S. I. Kiselev, J. C. Sankey, I. N. Krivorotov, N. C. Emley, R. J. Schoelkopf, R. A. Buhrman, and D. C. Ralph, Microwave oscillations of a nanomagnet driven by a spin-polarized current, Nature (London) **425**, 380 (2003).

[5] S. Sharma, B. Muralidharan, and A. Tulapurkar, Proposal for a domain wall nano-oscillator driven by non-uniform spin currents, Sci. Rep. **5**, 14647 (2015).

[6] A. Slavin and V. Tiberkevich, Nonlinear auto-oscillator theory of microwave generation by spin-polarized current, IEEE Trans. Magn. **45**, 1875 (2009).

[7] S. Tamaru, H. Kubota, K. Yakushiji, S. Yuasa, and A. Fukushima, Extremely coherent microwave emission from spin torque oscillator stabilized by phase locked loop, Sci. Rep. **5**, 18134 (2015).

[8] A. Bose, A. K. Shukla, K. Konishi, S. Jain, N. Asam, S. Bhuktare, H. Singh, D. D. Lam, Y. Fujii, S. Miwa, Y. Suzuki, and A. A. Tulapurkar, Observation of thermally driven field-like spin torque in magnetic tunnel junctions, Appl. Phys. Lett. **109**, 032406 (2016).

[9] S. Bhuktare, H. Singh, A. Bose, and A. A. Tulapurkar, Spintronic Oscillator Based on Spin-Current Feedback Using the Spin Hall Effect, Phys. Rev. Appl. **7**, 014022 (2017).

[10] M. M. Torunbalci, T. A. Gosavi, K. Y. Camsari, and S. A. Bhave, Magneto acoustic spin Hall oscillators, Sci. Rep. **8**, 1119 (2018).

[11] Swapnil Bhuktare, Arnab Bose, Hanuman Singh, and Ashwin A. Tulapurkar, Gyrator based on magneto-elastic coupling at a ferromagnetic/piezoelectric interface, Sci. Rep. **7**, 840 (2017).

[12] S. Bhuktare, A. Shukla, H. Singh, A. Bose, and A. A. Tulapurkar, Direct observation of the reciprocity between spin current and phonon interconversion, Appl. Phys. Lett. **114**, 052402 (2019).

[13] A. Bose, S. Bhuktare, H. Singh, S. Dutta, V. Achanta, and A. A. Tulapurkar, Direct detection of spin Nernst effect in Pt, Appl. Phys. Lett. **112**, 162401 (2018).

[14] A. Bose, A. S. Shukla, S. Dutta, S. Bhuktare, H. Singh, and A. A. Tulapurkar, Control of magnetization dynamics by spin-Nernst torque, Phys. Rev. B **98**, 184412 (2018).

[15] J. Torrejon, M. Riou, F. A. Araujo, S. Tsunegi, G. Khalsa, D. Querlioz, P. Bortolotti, V. Cros, K. Yakushiji, A. Fukushima, H. Kubota, S. Yuasa, M. D. Stiles, and J. Grollier, Neuromorphic computing with nanoscale spintronic oscillators, Nature **547**, 428 (2017).

[16] S. Kaka, M. R. Pufall, W. H. Rippard, T. J. Silva, S. E. Russek, and J. A. Katine, Mutual phase-locking of microwave spin torque nano-oscillators, Nature (London) **437**, 389 (2005).

[17] F. B. Mancoff, N. D. Rizzo, B. N. Engel, and S. Tehrani, Phase-locking in double-point-contact spin-transfer devices, Nature **437**, 393 (2005).

[18] J. Grollier, V. Cros, and A. Fert, Synchronization of spin-transfer oscillators driven by stimulated microwave currents, Phys. Rev. B **73**, 060409R (2006).

[19] A. Ruotolo, V. Cros, B. Georges, A. Dussaux, J. Grollier, C. Deranlot, R. Guillemet, K. Bouzehouane, S. Fusil, and A. Fert, Phase-locking of magnetic vortices mediated by antivortices, Nat. Nanotechnol. **4**, 528 (2009).

[20] S. Urazhdin, P. Tabor, V. Tyberkevych, and A. Slavin, Fractional Synchronization of Spin-Torque Nano-Oscillators, Phys. Rev. Lett. **105**, 104101 (2010).

[21] A. Dussaux, B. Georges, J. Grollier, V. Cros, A. V. Khvalkovskiy, A. Fukushima, M. Konoto, H. Kubota, K. Yakushiji, S. Yuasa, K. A. Zvezdin, K. Ando, and A. Fert, Large microwave generation from current-driven magnetic vortex oscillators in magnetic tunnel junctions, Nat. Commun. **1**, 8-1-6 (2010).

[22] M. Quinsat, J. F. Sierra, I. Firastrau, V. Tiberkevich, A. Slavin, D. Gusakova, L. D. Buda-Prejbeanu, M. Zarudniev, J.-P. Michel, U. Ebels, B. Dieny, M.-C. Cyrille, J. A. Katine, D. Mauri, and A. Zeltser, Injection locking of tunnel junction oscillators to a microwave current, Appl. Phys. Lett. **98**, 182503 (2011).

[23] A. Dussaux, A. V. Khvalkovskiy, J. Grollier, V. Cros, A. Fukushima, M. Konoto, H. Kubota, K. Yakushiji, S. Yuasa, K. Ando, and A. Fert, Phase locking of vortex based spin transfer oscillators to a microwave current, Appl. Phys. Lett. **98**, 132506 (2011).

[24] V. E. Demidov, H. Ulrichs, S. V. Gurevich, S. O. Demokritov, V. S. Tiberkevich, A. N. Slavin, A. Zholud, and S. Urazhdin, Synchronization of spin Hall nano-oscillators to external microwave signals, Nat. Commun. **5**, 3179 (2014).

[25] P. K. Muduli, Ye. Pogoryelov, F. Mancoff, and J. Åkerman, Modulation of individual and mutually synchronized nanocontact-based spin torque oscillators, IEEE Trans. Magn. **47**, 1575 (2011).

[26] S. Sani, J. Persson, S. M. Mohseni, Ye Pogoryelov, P. K. Muduli, A. Eklund, G. Malm, M. Kall, A. Dmitriev, and J. Åkerman, Mutually synchronized bottom-up multi-nanocontact spin-torque oscillators, Nat. Commun. **4**, 2731 (2013).

[27] A. Slavin and V. Tiberkevich, Theory of mutual phase locking of spin-torque nanosized oscillators, Phys. Rev. B **74**, 104401 (2006).

[28] H. Singh, K. Konishi, S. Bhuktare, A. Bose, S. Miwa, A. Fukushima, K. Yakushiji, S. Yuasa, H. Kubota, Y. Suzuki, and A. A. Tulapurkar, Integer, Fractional and Side Band Injection Locking of Spintronic Feedback Nano Oscillator to Microwave Signal, Phys. Rev. Appl. **8**, 064011 (2017).

[29] H. Singh, K. Konishi, S. Bhuktare, A. Bose, S. Miwa, A. Fukushima, K. Yakushiji, S. Yuasa, H. Kubota, Y. Suzuki, and A. A. Tulapurkar, Effect of external magnetic field on locking range of spintronic feedback nano oscillator, AIP Adv. **8**, 056010 (2018).

[30] S. Tsunegi, E. Grimaldi, R. Lebrun, H. Kubota, A. S. Jenkins, K. Yakushiji, A. Fukushima, P. Bortolotti, J. Grollier, S. Yuasa, and V. Cros, Self-injection locking of a vortex spin torque oscillator by delayed feedback, Sci. Rep. **6**, 26849 (2016).

[31] H. Singh, A. Bose, S. Bhuktare, A. Fukushima, K. Yakushiji, S. Yuasa, H. Kubota, and A. A. Tulapurkar, Self-Injection Locking of Spin Torque Nano Oscillator with Magnetic Field Feedback, Phys. Rev. Appl. **10**, 024001 (2018).

[32] A. Houshang, E. Iacocca, P. Dürrenfeld, S. R. Sani, J. Åkerman, and R. K. Dumas, Spin-wave-beam driven synchronization of nanocontact spin-torque oscillators, Nat. Nanotechnol. **11**, 280 (2016).

[33] A. Awad, P. Dürrenfeld, A. Houshang, M. Dvornik, E. Iacocca, R. K. Dumas, and J. Åkerman, Long-range mutual synchronization of spin Hall nano-oscillators, Nat. Phys. **13**, 292 (2017).

[34] N. Locatelli, A. Hamadeh, F. A. Araujo, A. D. Belanovsky, P. N. Skirdkov, R. Lebrun, V. V. Naletov, K. A. Zvezdin, M. Muñoz, J. Grollier1, O. Klein, V. Cros, and G. Loubens, Efficient synchronization of dipolarly coupled vortex-based spin transfer nano-oscillators, Sci. Rep. **5**, 17039 (2015).

[35] R. Lebrun, S. Tsunegi, P. Bortolotti, H. Kubota, A. S. Jenkins, M. Romera, K. Yakushiji, A. Fukushima, J. Grollier, S. Yuasa, and V. Cros, Mutual synchronization of spin torque nano-oscillators through a long range and tunable electrical coupling scheme, Nat. Commun. **8**, 15825 (2017).

[36] D. Dixit, K. Konishi, C. V. Tomy, Y. Suzuki, and A. A. Tulapurkar, Spintronic oscillator based on magnetic field feedback, Appl. Phys. Lett. **101**, 122410 (2012).

[37] D. Kumar, K. Konishi, Nikhil Kumar, S. Miwa, A. Fukushima, K. Yakushiji, S. Yuasa, H. Kubota, C. V. Tomy, A. Prabhakar, Y. Suzuki, and A. Tulapurkar, Coherent

microwave generation by spintronic feedback oscillator, Sci. Rep. **6**, 30747 (2016).

[38] O. J. Lee, P. M. Braganca, V. S. Pribiag, D. C. Ralph, and R. A. Buhrman, Quasilinear spin-torque nano-oscillator via enhanced negative feedback of power fluctuations, Phys. Rev. B **88**, 224411 (2013).

[39] J. M. Shaw, T. J. Silva, M. L. Schneider, and R. D. McMichael, Spin dynamics and mode structure in nanomagnet arrays: Effects of size and thickness on linewidth and damping, Phys. Rev. B **79**, 184404 (2009).

[40] See Supplemental Material at http://link.aps.org/supplemental/10.1103/PhysRevApplied.11.054028 for free-running frequency of MTJ as a function of applied external magnetic field and the design of synchronized arrays.

[41] M. I. Rabinovich, P. Varona, A. I. Selverston, and H. D. I. Abarbanel, Dynamical principles in neuroscience, Rev. Mod. Phys. **78**, 1213 (2006).

[42] W. T. Coffey, Yu. P. Kalmykov, and J. T. Waldron, *The Langevin Equation: With Applications to Stochastic Problems in Physics, Chemistry and Electrical Engineering* (World Scientific, Singapore, 2004), 2nd ed.